CORA Cork Open Research Archive
Cartlann Taighde Oscailte Chorcaí

Title	Modeling 1/f and Lorenzian noise in III-V MOSFETs
Authors	Caruso, Enrico;Bettetti, F.;Del Linz, L.;Pin, D.;Segatto, M.;Palestri, Pierpaolo
Publication date	2019-09-01
Original Citation	Caruso, E., Bettetti, F., Linz, L. D., Pin, D., Segatto, M. and Palestri, P. (2019) 'Modeling 1/f and Lorenzian noise in III-V MOSFETs', 2019 International Conference on Simulation of Semiconductor Processes and Devices (SISPAD), Udine, Italy, 4-6 Sept. doi: 10.1109/SISPAD.2019.8870548
Type of publication	Conference item
Link to publisher's version	https://ieeexplore.ieee.org/document/8870548 - 10.1109/SISPAD.2019.8870548
Rights	© 2019 IEEE. Personal use of this material is permitted. Permission from IEEE must be obtained for all other uses, in any current or future media, including reprinting/republishing this material for advertising or promotional purposes, creating new collective works, for resale or redistribution to servers or lists, or reuse of any copyrighted component of this work in other works.
Download date	2026-10-17 08:48:10
Item downloaded from	https://hdl.handle.net/10468/9167

UCC
University College Cork, Ireland
Coláiste na hOllscoile Corcaigh

Modeling 1/f and Lorenzian noise in III-V MOSFETs

E. Caruso*, F. Bettetti, L. Del Linz, D. Pin, M. Segatto, P. Palestri
*Tyndall National Institute, University College Cork, Cork, Ireland
DPIA, University of Udine, Via delle Scienze 206, 33100, Udine, Italy

***Abstract*— We present an approach to model 1/f and random telegraph noise in TCAD combining the models for non-local tunneling to traps and generation/recombination noise. The TCAD results are compared with simple numerical expression to understand the influence of the device and trap parameters on the noise spectrum. The simulation deck is then used to compute the low-frequency noise spectrum in III-V MOSFETs using traps distributions extracted from multi-frequency C-V measurements.**

Keywords—Lorenzian, 1/f, border traps, modelling, TCAD, noise

I. Introduction and Model description

1/f noise in MOSFETs has a significant impact on the performance of RF circuits such as oscillators and mixers due to up-conversion [1]. The power spectral density goes as the reciprocal of the area and so becomes critical with device scaling. Furthermore, for short channel devices single traps increase the variability of the noise spectrum and result in random-telegraph noise (RTN) [2][3].
Models for 1/f noise are usually based on the assumption of uniform trap distribution over space and energy in the gate oxide [4][5] while multi-frequency C-V and G-V experiments [6] have shown complex border traps distributions in high-*k* dielectrics.

We use TCAD simulations [7] implementing the model for generation/recombination noise of [8]. Coupled with the non-local model tunneling to and from traps, our approach describes the carrier number fluctuations due to trapping/de-trapping in the gate insulator with arbitrary energy and space distributions of donors and acceptors. Mobility fluctuations [5] are not accounted for by the present implementation.

II. Results for uniform trap distribution

Before considering complex trap distributions, we validate our approach by comparing the simulation results with the prediction of the well known formula for drain current noise due to carrier number fluctuation [4]:

$$S_{Id}(f) = \frac{q^2 KT g_m^2 N_{BT}}{\alpha_t W L C_{OX}^2 f} \tag{1}$$

N_{BT} is the concentration of traps per unit volume and unit energy. The transconductance g_m is extracted from the I-V curves. The factor $\alpha_t = (2/\hbar)\sqrt{2m_{eff}\phi_B}$ is computed using the TCAD tunneling mass (m_{eff}) and barrier (ϕ_B) between semiconductor and insulator.

Fig. 1 compares Eq. 1 and TCAD results for Si/SiO_2 and $In_{0.53}Ga_{0.47}As/Al_2O_3$ large area MOSFETs at low V_{DS}. The noise is larger in the $In_{0.53}Ga_{0.47}As$ device due to the larger mobility (we used bulk mobility just to simplify the comparison with the analytical model).

The agreement between Eq. 1 and the TCAD results is very good and somewhat surprising: Eq. 1 is obtained assuming that the tunneling rate decreases exponentially when penetrating into the oxide and that the decay rate is the same for all energies, i.e. $P_{tun}=exp(-\alpha_t x)$. On the other hand, in TCAD the devices show a triangular tunneling barrier and, furthermore, the trapping rate depends on energy [7]. This point will be discussed in the next section.

Fig. 2 shows the effect of the gate bias on the spectrum, considering elastic and inelastic tunneling. Above threshold (not shown) all curves stay very close (same g_m), while below threshold we see a decrease of the current spectrum. This decrease is even larger when only elastic tunneling is used: in such case, there are very few electrons at the interface able to tunnel into the traps. We thus propose a correcting factor to Eq. 1 in order to reproduce the TCAD results:

$$S_{Id}(f) = \frac{q^2 KT g_m^2 N_{BT}}{\alpha_t W L C_{OX}^2 f} \frac{1}{1+\exp(-\frac{qE_F}{KT})} \tag{2}$$

where E_F is the distance between the Fermi level and the conduction band minimum at the interface. Eq. 2 captures the decrease of S_{Id} at low V_{GS} for elastic traps.

III. Interpretation with numerical models

To understand why Eq. 1 hold also with triangular tunneling barrier, we have worked out the different dependences related to the tunneling probability and trap capture/emission rates and see that they tend to compensate each other. First of all, we model the fluctuation of the trap occupation due to elastic tunneling with a Lorentzian function with inverse time constant:

$$\frac{1}{\tau} = \frac{\sqrt{8m_{eff}}m_0 g_c V_T}{\hbar^4 \pi} E_T^2 \sqrt{\phi_B - E_T} P_{tun} \tag{3}$$

where the meaning of the terms and the energy references can be seen in Fig. 3 and g_C=1. The expression is the same used in [7] for elastic tunneling into traps. The tunneling probability P_{tun} across the trapezoidal barrier is computed with WKB approximation from x=0 to x_T. Ramo's theorem is used to compute the current fluctuation induce by the trap as qv/L. At low V_{DS} the velocity is the mobility μ multiplied by V_{DS}/L. We thus get:

$$S_{Id}(f) = \left(\frac{q\mu V_{DS}}{L^2}\right)^2 4 f_T (1 - f_T) \frac{\tau}{1+(2\pi f \tau)^2} \tag{4}$$

where f_T is the trap distribution (Fermi-Dirac statistic). Fig. 4 compares Eq. 4 with TCAD results: the agreement is quite good and tends to be almost perfect when using T_{OX}>30nm (not shown) where the assumption of the Ramo weighting field equal to *1/L* is more appropriated. The noise is larger for V_{GS} values such that the trap energy gets aligned with the Fermi level.

When considering multiple traps, Eq. 4 should be integrated on the trap distribution:

978-1-7281-0940-4/19/$31.00 ©2019 IEEE

$$S_{Id}(f) = \left(\frac{q\mu V_{DS}}{L^2}\right)^2 WL \iint N_{BT} \frac{4f_T(1-f_T)\tau}{1+(2\pi f\tau)^2} dE_T dx_T \quad (5)$$

where f_T, τ and N_{BT} depend on the trap position and energy. If N_{BT} is constant over energy and space, and the electric field in the oxide is almost null, we get $\tau=\tau_0 \exp(\alpha_t x_T)$ and Eq. 5 leads to Eq. 2.

Fig. 5 compares Eq. 5 with TCAD results for a case with F_{OX}=1.44 MV/cm. We see that even if the oxide field is not null, the agreement between Eq. 5 and Eq. 2 is very good. We have verified that this holds even for higher F_{OX}. Differences between Eq. 5 and Eq. 2 appear for example at 7 MV/cm as in Fig. 6. The influence of F_{OX} is thus visible only at low frequency and makes S_{Id} deviate from the 1/f behavior.

In addition, from Figs. 5 and 6 we see that the agreement between Eq. 5 and the TCAD results is good, in line with Figs. 1 and 2. It improves when using T_{OX}>30 nm (not shown) for the same reasons discussed for Fig. 4.

To motivate the weak influence of F_{OX} on the results, we first simplify the problem by noticing that $f_T(1-f_T)$ resembles a Dirac-delta at energy E_F. We thus can eliminate the integral over energy in Eq. 5 and get:

$$S_{Id}(f) = \left(\frac{q\mu V_{DS}}{L^2}\right)^2 WL4KT \int N_{BT} \frac{\tau}{1+(2\pi f\tau)^2} dx_T \quad (6)$$

Where τ and N_{BT} are compute for the E_T level aligned with E_F. Fig. 5 shows that the Eq. 6 is very close to Eq. 5 over the whole frequency range. Differences between Eq. 5 and Eq. 6 appear at high F_{OX} as can be seen in Fig. 6, but in any case Eq. 6 is a good starting point for a simplified analysis.

Fig. 7 plots the term $\tau/[1+(2\pi f\tau)^2]$ inside the integral of Eq. 6 for 3 different F_{OX} values: the shape of the curves and their integral is the same for 1MV/cm and 7 MV/cm. The function indeed peaks at $\tau=1/(2\pi f)$ with a peak value of $1/(4\pi f)$; for large F_{OX} the tunneling probability (Fig. 8) increases with respect to the simple exponential term related to rectangular barrier, reducing τ and moving the peak of $\tau/[1+(2\pi f\tau)^2]$ further inside the oxide. When F_{OX} is too large, the function $\tau/[1+(2\pi f\tau)^2]$ gets cut off because there is no position where $\tau=1/(2\pi f)$, as can be seen in Fig. 7 for the case with F_{OX}=9 MV/cm and the integral is lower than at low F_{OX}. Note that in Fig. 7 we see a weaker effect of F_{OX} compare to Fig. 6. This is due to the fact that in Fig. 7 we set a fixed E_F=0.1 eV while in Fig. 6 the high F_{OX} is associated to a large E_F due to the low DoS of the channel material. The energy of the tunneling path is thus higher in Fig. 6 and the classical turning point is moved to the left compared to. Fig. 7.

IV. Realistic Trap Distribution

We now consider a realistic trap distribution obtained by fitting multi-frequency C-V (Fig. 9a) and G-V (not shown) curves for InGaAs/Al_2O_3 capacitors [6]. The acceptor and donor profiles (plots b and c) are not uniform in energy and are positioned close to the interface. The resulting noise spectra at different biases are reported in Fig. 10. In strong inversion, tunneling is more localized and takes place with traps closer to the interface. Since 1/f noise is the combination RTN over the different tunneling rates, this results in a flat spectra up to a knee frequency related to the slowest tunneling rate. Above that, we have 1/f dependence. In accumulation, instead, the slowest tunneling rate is much smaller and we see 1/f noise even at low frequency, tending to $1/f^2$ when approaching the largest tunneling rate.

We now consider the influence of an additional uniform trap distribution inside the oxide. This additional charge does not affect the C-V curves simulated in Fig. 9 up to $N_{BT} \sim 10^{19}$ $cm^{-3}eV^{-1}$, and thus is out of the detection limit of the multi-frequency C-V experiment (from 1 kHz up to 1 MHz). Fig. 11 shows that this additional contribution results in 1/f noise at low frequency in inversion, demonstrating that low-frequency noise measurements can probe traps deep in the oxide that are not probed by C-V at typical frequency range of measurement (1 kHz up to 1 MHz). Fig. 12 shows that the impact of bulk traps is much weaker in depletion/accumulation, where the D_{BT} is higher and goes deeper into the oxide than in inversion (Fig. 9 b-c), so that the additional uniform N_{BT} does not play a significant role.

V. Conclusions

We have shown that TCAD simulations can be used to analyze low frequency noise in MOSFETs considering complex trap distributions. The simple formula for carrier number fluctuation holds also when the tunneling barrier is not rectangular and the trapping rate changes with energy. On the other hand, a correction to that formula has been proposed to describe the lower of the noise due to elastic tunnel in the subthreshold regime.

Acknowledgment

The authors would like to thank Paolo Scarbolo, Luca Selmi and Paul Hurley for many helpful discussions and encouragement.

References

[1] T.Lee, “The Design of CMOS Radio-Frequency Integrated Circuits”, Cambridge university press, 2003

[2] H. Tuinhout and A. Z. Duijnhoven, “Evaluation of 1/f noise variability in the subthreshold region of MOSFETs", Conf. Proc. ICMTS, pp. 87-92, 2013

[3] M. Si, N. J. Conrad, S. Shin, J. Gu, J. Zhang, M. A. Alam and P. D. Ye, "Low-Frequency Noise and Random Telegraph Noise on Near-Ballistic III-V MOSFETs", IEEE Trans. Electron Devices, vol. 62, no. 11, pp. 3508-3515. 2015

[4] S.ChristenssonI, Lundström and C.Svensson, “Low frequency noise in MOS transistors—I theory”, Solid-State Electronics, vol. 11, no. 9, pp. 797-812. 1968

[5] G. Ghibaudo, O. Roux, Ch. Nguyen ‐ Duc, F. Balestra and J. Brini, "Improved analysis of low frequency noise in field ‐ effect MOS transistors", Phys. Stat. Sol. (a), vol. 124, no 2, pp. 571-581, 1991

[6] E. Caruso, J. Lin, K. F. Burke, K. Cherkaoui, D. Esseni, F. Gity, S. Monaghan, P. Palestri, P. Hurley and L. Selmi, "Profiling border-traps by TCAD analysis of multifrequency CV-curves in Al_2O_3/InGaAs stacks," Conf. Proc. EUROSOI-ULIS, pp. 1-4, 2018

[7] Synposys Inc., Sentaurus DeviceTM, v. L-2016.03-SP2, 2016

[8] F. Bonani and G. Ghione. "Generation–recombination noise modelling in semiconductor devices through population or approximate equivalent current density fluctuations", Solid-State Electronics, vol. 43, no. 2, 1999

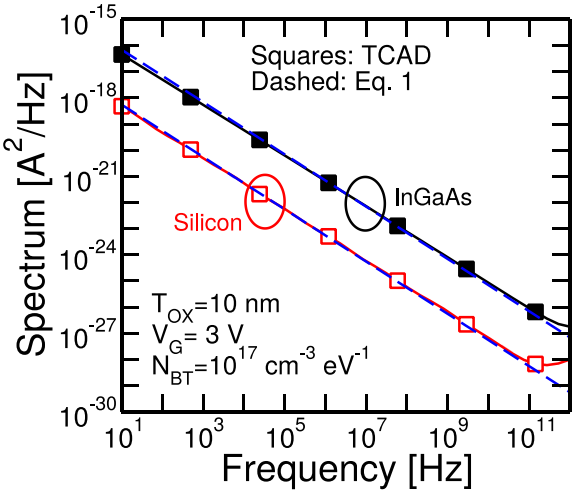

Figure 1 Comparison between the TCAD simulations employ an inelastic tunneling model for traps, using a trap volume V_T=10^{-11} µm^3 and a phonon energy E_{ph}=48 meV. W= 1 µm, L=0.2 µm, V_{DS}=25 mV.

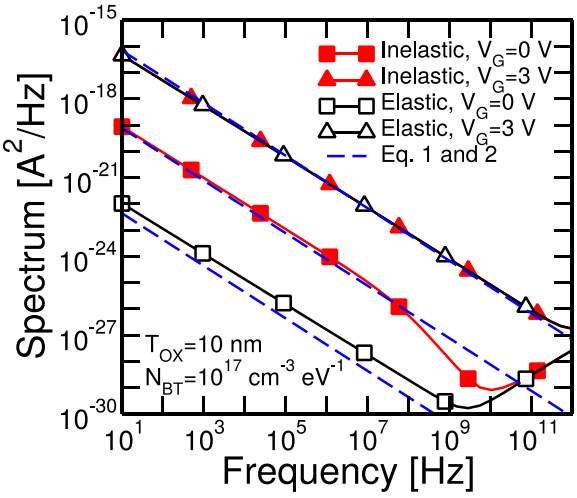

Figure 2 Comparison between TCAD simulations and the analytic model of Eq. 1-2 (dashed line) for an InGaAs/Al_2O_3 MOSFET simulated at 0 V (squares) and 3 V (triangles). TCAD simulations use inelastic (closed symbols) and elastic (open symbols) tunneling models for traps.

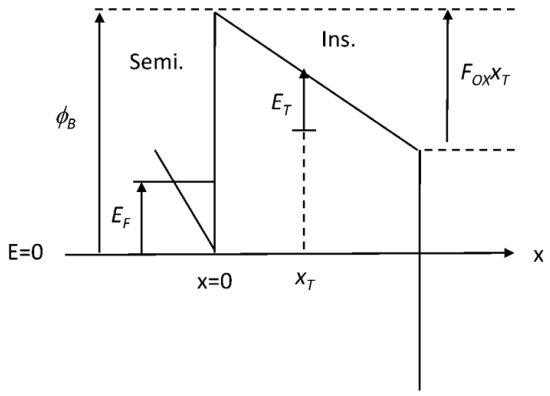

Figure 3 Band-diagram of the semiconductor/insulator system in the case of a single trap. The energy reference is the bottom of the conduction band at the interface.

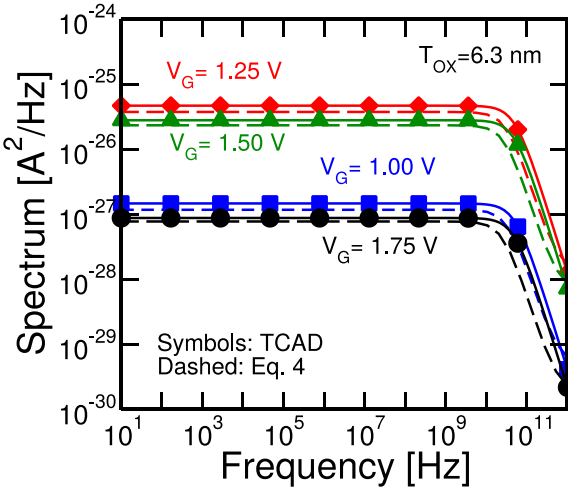

Figure 4 Comparison between the analytical model based on Eqs.3,4 and TCAD simulations for a single trap at x_T=1nm from the interface with an energy E_T=3.05eV. Device parameters are the same as in Fig.1 (InGaAs device) excpet for T_{OX}=6.3nm.

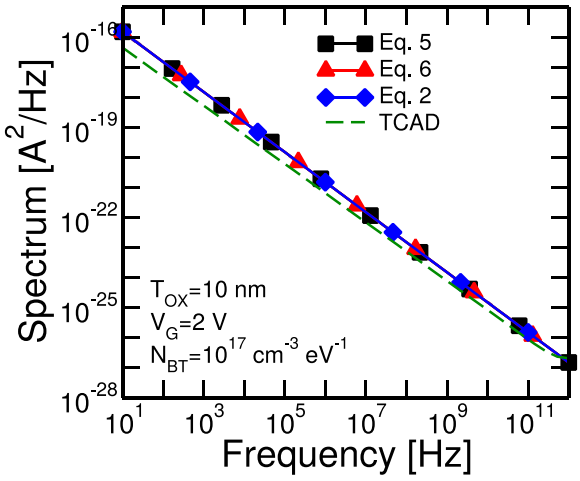

Figure 5 Comparison between the various numerical models and TCAD simulations for distributed traps and F_{OX}=1.44 MV/cm. The device is the same as in Fig.1 (InGaAs device) but an uniform trap distribution with N_{BT}=10^{17} cm^{-3}eV^{-1} is used.

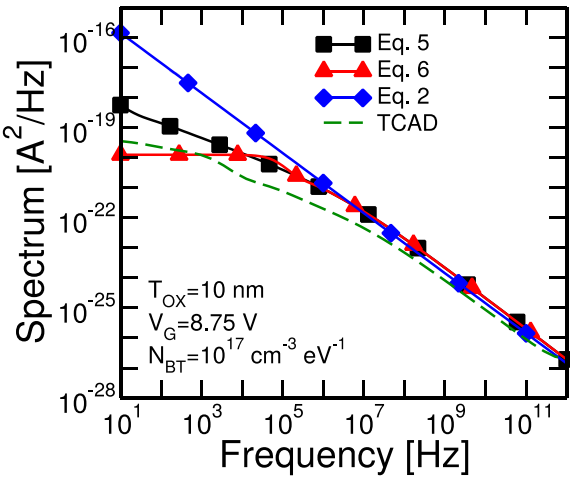

Figure 6 Comparison between the various numerical models and TCAD simulations for distributed traps and F_{OX}=7 MV/cm. The device is the same as in Fig.1 (InGaAs device) but an uniform trap distribution with N_{BT}=10^{17} cm^{-3}eV^{-1} is used.

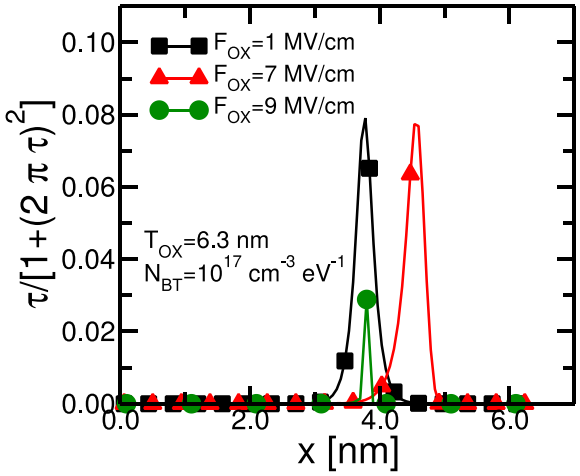

Figure 7 Term $\tau/[1+(2\pi f\tau)^2]$ evaluated inside the insulator for an energy equal to the Fermi level in the substrate (set to 0.1eV). The frequency is set to f=1Hz.

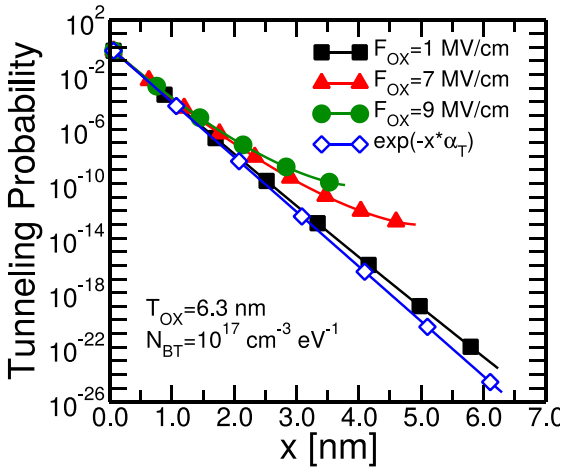

Figure 8 Tunneling probability along the path of Figure 7 for differernt values of the oxide field F_{OX}.

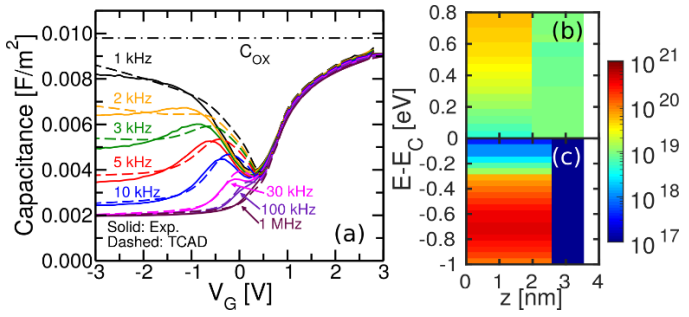

Figure 9 Experimental (solid lines) multi-frequency C-V (a) compared with simulated data (dashed lines). Simulations use (b) acceptor and (c) donor $D_{BT}(z,E)$ inside the 6.3 nm Al_2O_3. Doping is $N_D=3.0\cdot10^{17}$ cm^{-3} and SRH time is τ_g=80 ps. The energy distributions are referred to the InGaAs conduction band (E_C).

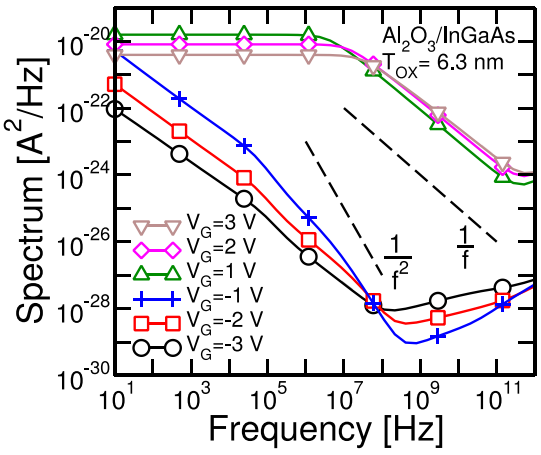

Figure 10 Noise spectrum at different V_G using the $D_{BT}(z,E)$ of Fig. 9. W= 1 µm, L=0.2 µm, V_{DS}=25 mV.

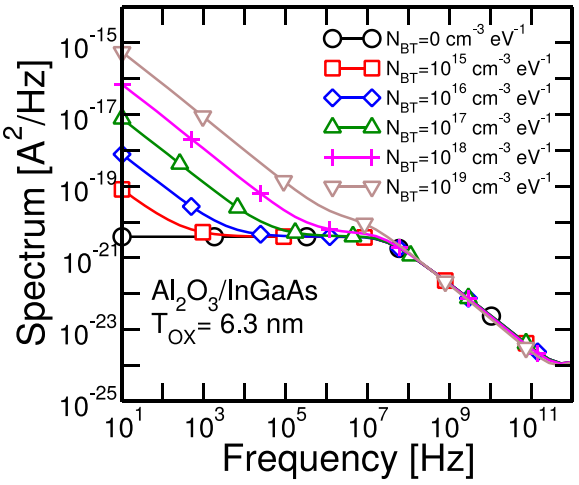

Figure 11 Noise spectrum using a border traps distribution obtained from the sum of the $D_{BT}(z,E)$ in Fig. 9 and an additional uniform acceptor distribution with density N_{BT}. In all simulations V_{GS} is 3 V, except for the one with $N_{BT}=10^{19}$ cm^{-3} eV^{-1}, where V_{GS} is 5 V to compensate for the threshold shift due to the traps.

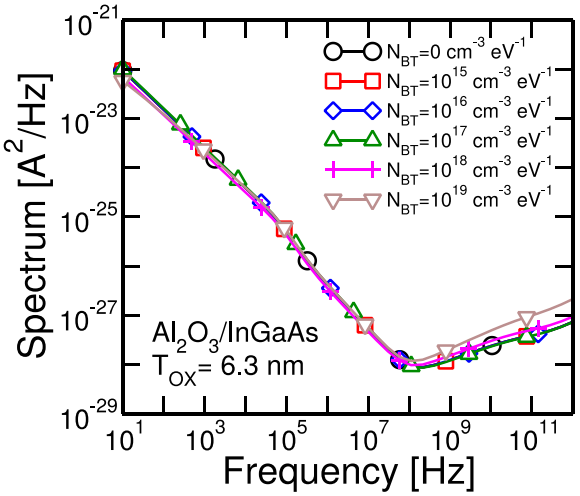

Figure 12 Noise spectrum using a border traps distribution obtained from the sum of the $D_{BT}(z,E)$ in Fig. 9 and an additional uniform donor distribution with density N_{BT}. The spectrum is extracted at the same E_C-E_F=-0.5 eV (corresponding to negative V_{GS}).